

A Measurement of the Hubble Constant using Gravitational Waves from the Binary Merger GW190814

SERGIY S. VASYLYEV^{1,2} AND ALEXEI V. FILIPPENKO^{1,3}

¹*Department of Astronomy, University of California, Berkeley, CA 94720-3411, USA*

²*Steven Nelson Graduate Fellow*

³*Miller Senior Fellow, Miller Institute for Basic Research in Science, University of California, Berkeley, CA 94720, USA*

ABSTRACT

We present a test of the statistical method introduced by Bernard F. Shutz in 1986 using only gravitational waves to infer the Hubble constant (H_0) from GW190814, the first high-probability neutron-star–black-hole (NS–BH) merger candidate detected by the Laser Interferometer Gravitational-wave Observatory (LIGO) and the Virgo interferometer. We apply a baseline test of this method to the binary neutron star (BNS) merger GW170817 and find $H_0 = 70^{+35.0}_{-18.0} \text{ km s}^{-1} \text{ Mpc}^{-1}$ (maximum *a posteriori* and 68.3% highest density posterior interval) for a galaxy B -band luminosity threshold of $L_B \geq 0.001 L_B^*$ with a correction for catalog incompleteness. Repeating the calculation for GW190814, we obtain $H_0 = 67^{+41.0}_{-26.0} \text{ km s}^{-1} \text{ Mpc}^{-1}$ and $H_0 = 71^{+34.0}_{-30.0} \text{ km s}^{-1} \text{ Mpc}^{-1}$ for $L_B \geq 0.001 L_B^*$ and $L_B \geq 0.626 L_B^*$, respectively. Combining the posteriors for both events yields $H_0 = 70^{+29.0}_{-18.0} \text{ km s}^{-1} \text{ Mpc}^{-1}$, demonstrating the improvement on constraints when using multiple gravitational-wave events. We also confirm the results of other works that adopt this method, showing that increasing the L_B threshold enhances the posterior structure and slightly shifts the distribution’s peak to higher H_0 values. We repeat the joint inference using the low-spin PhenomPNRT (Abbott et al. 2019a) and the newly available combined (SEOBNRv4PHM + IMRPhenomPv3HM; Abbott et al. 2020) posterior samples for GW170817 and GW190814, respectively, achieving a tighter constraint of $H_0 = 69^{+29.0}_{-14.0} \text{ km s}^{-1} \text{ Mpc}^{-1}$.

Keywords: Hubble constant — gravitational waves — neutron stars — black holes

1. INTRODUCTION

Gravitational-wave (GW) and electromagnetic (EM) follow-up observations of black hole (BH) and neutron star (NS) mergers provide a novel method of probing dense astrophysical environments and enable a unique channel for cosmology. The August 2017 discovery of NS–NS merger GW170817 by the Laser Interferometer Gravitational-Wave Observatory (LIGO) and the Virgo interferometer, as well as the subsequent multimessenger observations by the coordination of thousands of astronomers, has brought forth a new era of astronomy (Abbott et al. 2017a). Two weeks after this discovery, the LIGO detectors in Hanford, Washington and Livingston, Louisiana, as well as the newly added Virgo detector in Italy, ceased operation for upgrades, marking the end of Observing Run 2 (O2). The analysis of GW170817 covered the entire EM spectrum, giving insights into the generation of short-duration gamma-ray bursts (sGRBs; Goldstein et al. 2017), general relativity in the strong-gravity regime (Abbott et al. 2019b), the production of r -process elements (Kasen et al. 2017), constraints on the NS equation of state (Annala et al. 2018), and an independent measurement of the Hubble constant H_0 (Abbott et al. 2017b).

Observing Run 3 (O3) began in late April of 2019, promising a higher rate of GW detections owing to sensitivity upgrades to the three detectors. The search volume increased by $\sim 100\%$ from O2 to O3 according to Table 2 in KAGRA Collaboration, LIGO Scientific Collaboration, and Virgo Collaboration et al. (2018), thereby allowing for a significantly deeper survey. The end of O3 was initially planned for April 30, 2020 in order to conduct additional upgrades, but O3 was ended prematurely on March 27, 2020 because of the COVID-19 pandemic. In summary, O3 produced 36 BH–BH mergers, 1 NS–NS merger, and the first-ever candidate NS–BH merger (GW190814) with at least 90% confidence. In this paper, we will focus on the candidate NS–BH merger GW190814, as its exquisite localization (see Section 2.3) makes it a prime object for the statistical inference of H_0 described below. Hereinafter, we will refer to GW190814 as a NS–BH merger, though we acknowledge that this event has not been explicitly shown to be a NS–BH; it likely contains compact objects with a mass range falling within the criterion for a NS–BH merger.¹

¹ See LVC Public Alerts User Guide’s criteria for GW event classification

1.1. The Hubble Tension

Recent measurements of H_0 reveal at least a 4.2σ tension. The *Planck* satellite team infers $H_0 = 67.4 \pm 0.5 \text{ km s}^{-1} \text{ Mpc}^{-1}$ using cosmic microwave background (CMB) data and assuming the standard Λ -CDM model is correct (Planck Collaboration et al. 2018). The SH0ES (Supernovae, H_0 , for the Equation of State of Dark Energy) team measured $H_0 = 74.03 \pm 1.42 \text{ km s}^{-1} \text{ Mpc}^{-1}$ with an independent method, combining Cepheid-variable calibrations with luminosity distance measurements of Type Ia supernovae (Riess et al. 2018, 2019). The SH0ES method is sensitive to how well the distance ladder is calibrated. Other recent studies have only enhanced the discrepancy between the two methods mentioned above, for a combined tension of $\sim 6\sigma$ (Riess 2020). For example, the HOLiCOW (H_0 Lenses in COSMOGRAILs Wellspring) and STRIDES (STRong-lensing Insights into Dark Energy Survey) teams use measured time delays in the light curves of different images of single strongly lensed quasars to obtain $H_0 = 73.3 \pm 1.8 \text{ km s}^{-1} \text{ Mpc}^{-1}$ and $H_0 = 74.2 \pm 1.4 \text{ km s}^{-1} \text{ Mpc}^{-1}$, respectively, agreeing with the SH0ES measurement (Wong et al. 2019; Shajib et al. 2020). Other measurements that broadly agree with the SH0ES value include the tip of the red giant branch (Jang & Lee 2017; Hatt et al. 2018, TRGB1, TRGB2;), Mira variables (Huang et al. 2020), surface brightness fluctuations (SBF), and masers (Verde et al. 2019). On the other hand, measurements from big-bang nucleosynthesis and baryon acoustic oscillations (BBN + BAO; Cuceu et al. 2019), Wilkinson Microwave Anisotropy Probe (WMAP) CMB + BAO (Hinshaw et al. 2009), Atacama Cosmology Telescope Polarization camera (ACTPol) + BAO (Louis et al. 2017), and the South Pole Telescope SZ camera (SPT-SZ) + BAO (Story et al. 2013) favor the *Planck* result.

1.2. The Standard-Siren Method

The above tension between local (SH0ES, etc.) and early-universe (*Planck*) measurements of H_0 may be the result of underlying systematic effects or astrophysical causes. A new independent method using gravitational-wave sources as “standard sirens,” first proposed by Schutz (1986), could reconcile this discrepancy. This method uses the observed amplitude and the frequency of the gravitational waveform (from which a distance is determined) together with the measured redshift of the source’s host galaxy to infer H_0 (Holz & Hughes 2005; Nissanke et al. 2010; Vitale & Chen 2018; Mortlock et al. 2019). Standard sirens do not need a distance ladder and are thereby decoupled from systematic effects that may be introduced in methods relying on it.

The true host galaxy can only be identified with an EM counterpart. GW170817 produced an optical transient powered by radioactive decay, called a kilonova (Kasen et al. 2017). The source’s host galaxy was identified as NGC 4993

at a luminosity distance of $40_{-14.0}^{+8.0} \text{ Mpc}$ (Coulter et al. 2017; Soares-Santos et al. 2017; Valenti et al. 2017; Arcavi et al. 2017; Tanvir et al. 2017; Lipunov et al. 2017). Abbott et al. (2017b) presented the first result using the standard siren method, estimating $H_0 = 70.0_{-8.0}^{+12.0} \text{ km s}^{-1} \text{ Mpc}^{-1}$.

1.3. The Galaxy-Catalog Method

BH-BH mergers are not expected to produce an optical transient, unlike NS-NS mergers. Some theoretical models suggest that NS-BH mergers may only produce a counterpart under certain physical conditions (Foucart et al. 2018, 2019; Barbieri et al. 2020). However, cosmological inferences are still possible without the EM counterpart.

The LIGO-Virgo detectors produce a sky map that constrains the location of a GW source to specific patches in the sky. Using a statistical approach (the catalog method), one can consider every galaxy in the source’s localization region as a potential host with some probability. Summing the probability assigned to each galaxy builds the full posterior on H_0 . Chen et al. (2018) show that an H_0 inference from GW sources with optical counterparts will converge faster than for dark sirens. Although using a so-called “dark siren” will not provide as precise a measurement from a single event compared to the case when the host galaxy is known, many more BH-BH mergers (dark sirens) are expected than NS-NS mergers (Baibhav et al. 2019), providing a useful validation test of the optical-counterpart method. Furthermore, combining several measurements will yield increasingly tighter constraints on H_0 (Chen et al. 2018; Nair et al. 2018; Feeney et al. 2019).

The galaxy catalog (statistical) method was first tested on simulated data by Del Pozzo (2012). More recently, Fishbach et al. (2019) used this method to infer H_0 from GW170817 without relying on the EM counterpart. They obtain several estimates for H_0 using various luminosity cuts and weighting schemes to galaxies in the GLADE 2.3 catalog described in Section 2.2. An estimate of H_0 from BH-BH merger GW170814 using a similar statistical method was recently obtained by the Dark Energy Survey (DES) Year-3 data team with a proprietary galaxy catalog (DES Y3; Abbott et al. 2018). The DES team computed $H_0 = 75_{-32.0}^{+40.0}$ and $H_0 = 78_{-24.0}^{+96.0} \text{ km s}^{-1} \text{ Mpc}^{-1}$ for the uniform prior ranges [20, 140] and [10, 220] $\text{km s}^{-1} \text{ Mpc}^{-1}$, respectively (Soares-Santos et al. 2019). The LIGO-Virgo Collaboration (LVC) combined high-probability BH-BH (dark sirens) from the O1 and O2 runs together with the GW170817 optical counterpart, yielding a joint value $H_0 = 68_{-7.0}^{+14.0}$ with a [20, 140] $\text{km s}^{-1} \text{ Mpc}^{-1}$ flat-in-log H_0 prior defined in Section 2.1 (Abbott et al. 2019c). This work also explored the effects of galaxy luminosity weighting on the H_0 posterior shape.

1.4. GW190814

On 2019-08-14, at 21:10:39 UT, LIGO Hanford, LIGO Livingston, and Virgo detected the GW event GW190814 with a false-alarm rate (FAR) of approximately 1 per 10^{25} yr at a luminosity distance of 267 ± 52 Mpc (LIGO Scientific Collaboration & Virgo Collaboration 2019). Although the NS-BH candidate GW190814 did not have an associated EM counterpart, we can still use the gravitational-wave data to produce meaningful results. Analysis by Abbott et al. (2020) showed that the primary and secondary masses of GW190814 are $23_{-1.0}^{+1.1} M_\odot$ and $2.59_{-0.09}^{+0.08} M_\odot$, respectively. The secondary mass approaches the observational MassGap ($3\text{--}5 M_\odot$), in which there is uncertainty regarding whether the object is the heaviest neutron star or the lightest black hole ever discovered. This should not affect our results, given our generous prior on the NS mass for the event. After initial submission of this paper, Abbott et al. (2020) performed the statistical method for GW190814 also using the GLADE catalog to obtain $H_0 = 75_{-13.0}^{+59.0} \text{ km s}^{-1} \text{ Mpc}^{-1}$ with a flat H_0 prior on $[20, 140] \text{ km s}^{-1} \text{ Mpc}^{-1}$ and using posterior samples.

We follow the methodology presented by Chen et al. (2018), Gray et al. (2019), and Abbott et al. (2019c) to obtain the H_0 posterior. With this paper we test the statistical method on a new GW-type candidate (NS-BH) and improve the accessibility of the gwcosmo² code. See the Appendix for a detailed discussion of the mathematics involved.

2. METHODS

Using the publicly available gwcosmo code, we construct a posterior on the Hubble constant using only gravitational waves for the NS-BH merger candidate GW190814. We use the Bayesian framework presented by Chen et al. (2018) and Gray et al. (2019), which is detailed in the Appendix. We outline our methodology starting with a thorough account of our assumed priors and input parameters used in gwcosmo. Note that we adopt the O2-H0 branch to perform these calculations, as it is the most stable at the time of writing.³ The preparation and injection of the GLADE 2.0 galaxy catalog is discussed in Section 2.2. The HEALPIX localization skymaps used for all of the calculations are described in Section 2.3. We create a baseline test of our assumptions by comparing to Abbott et al. (2019c) and Fishbach et al. (2019) using GW170817. We then explore parameter space to present multiple H_0 calculations for GW190814.

² <https://git.ligo.org/lscsoft/gwcosmo/-/tree/master>

³ We fix a few small syntax errors that prevented the code from running. Also, we add a few lines of code to gwcosmo.py and to the gwcosmo-single-posterior script to import NS-BH merger priors. The bin size of the “dl” array in skymap.marginalized_distance is changed from 200 to 50 for optimization reasons. The effect on our results is insignificant.

2.1. Priors and Input Parameters

Our analysis is carried out with both a uniform and “flat log prior” on H_0 over a set of different intervals. We use the definition for the flat log prior $p(H_0) \propto H_0^{-1}$ (Abbott et al. 2019c). Below, we describe the options passed to the *gwcosmo_single_posterior* script in the gwcosmo code. The italicized items are presented in Table 1.

1. The *mass distribution* is chosen to be either (a) BNS-uniform, a binary neutron star distribution over the interval $[1.0 M_\odot, 3.0 M_\odot]$, (b) BNS-Gaussian, a symmetric Gaussian distribution centered on $\mu = 1.35 M_\odot$ with $\sigma = 0.15 M_\odot$ (Kiziltan et al. 2010), and (c) NSBH-uniform, a uniform neutron-star–black-hole distribution with a uniform NS mass distribution over $[1 M_\odot, 3 M_\odot]$ and a power-law BH mass distribution over $[5 M_\odot, 40 M_\odot]$. The uniform component follows $p(m_2) = \text{constant}$, while the power-law component takes the form $p(m_1) \propto m_1^{-\alpha}$, with the power-law index $\alpha = 1.6$. Here, m_2 is the secondary (NS) mass and m_1 is the primary (BH) mass.
2. The *power spectral density (PSD)* parameter is associated with the detector sensitivity during either the O1, O2, or O3 observing runs (we choose O2 for GW170817 and O3 for GW190814).
3. The *completeness* parameter is defined as the ratio of the number of galaxies in a chosen galaxy catalog to the true number of galaxies in the cosmological volume. We discuss this in more detail in Section 2.2. and in the Appendix. Gray et al. (2019) study the effects of this parameter on the H_0 posterior extensively on simulated merger data in Sections III and IV.
4. *Galaxy weighting* may be set to either “False” (equal weights) or have *B*-band luminosity-dependent weights $\omega_i \propto L_B^i$. A luminosity-dependent weighting scheme follows the assumption that BH and NS merger rates scale with star-formation rates (Fong & Berger 2013).
5. *Luminosity threshold* gives the minimum *B*-band luminosity considered for the calculation; this parameter will be explored in depth in Section 3.

We hold the following parameters constant throughout every calculation.

1. *Linear cosmology* is set to “False” because we include galaxies with redshift $z > 0.1$.
2. *Posterior samples* is set to “False”, given that initially, at the time of writing this paper, there had not yet been a data release from the LIGO-Virgo Collaboration (LVC) for event GW190814. After submission of this paper, the LVC released the full posterior samples for GW190814,

allowing us (upon revision) to properly account for biases introduced by the approximation described below. Results for the latter analysis are found in Section 3.2. When neither a posterior sample nor an EM counterpart is used, the three-dimensional (3-D) skymap (see Section 2.3) is passed as the gravitational-wave data to the `skymap.marginalized_distance` function in `gwcosmo`, which is a Gaussian approximation to the GW’s distance posterior.

3. `Basic_pdet` is set to “False” allowing us to take into account redshifted mass, $M_z = M(1+z)$ (Chen et al. 2019).
4. The `uncertainty` parameter is set to “True,” taking into account the Gaussian uncertainties in redshift for each galaxy (see Section 2.2).
5. The `rate_evolution` parameter is set to “False,” which describes a constant merger rate $R(z)$ as it appears in Equation 11 of Abbott et al. (2019c). We assume the Λ CDM model ($\Omega_m = 0.308$, $\Omega_\Lambda = 0.692$). The effect of choosing a merger rate with a dependence on redshift is shown extensively by Abbott et al. (2019c).

2.2. Using the GLADE Galaxy Catalog

We use the GLADE v2.3 galaxy catalog throughout, adopting the parameters $\phi^* = 1.6 \times 10^{-2} h^3 \text{Mpc}^{-3}$, where $h = 0.7$ and $\beta = -1.07$ for the Schechter B -band luminosity function,

$$\rho(x)dx = \phi^* x^\beta e^{-x} dx, \quad x = L_B/L_B^*, \quad (1)$$

where $\rho(x)$ is the number density of galaxies and the characteristic B -band luminosity L_B^* corresponds to an absolute magnitude $M_B = -20.47$ (Gehrels et al. 2016).

The GLADE galaxy catalog contains nearly 3 million galaxies and is complete up to 300 Mpc at $L_B = 0.626 L_B^*$, corresponding to the median of the luminosity function (Arcavi et al. 2017). The statistical method is sensitive to the galaxy completeness fraction, f (Gray et al. 2019). The Glade catalog’s high completeness fraction over the redshifts considered for this study provides a significant advantage over other catalogs (Dlya et al. 2018). Approximately half of the objects in the catalog have a measured B -band luminosity.

All redshifts in GLADE are corrected for peculiar motions and are in the heliocentric frame (Carrick et al. 2015). In order to correct for radial group velocities, we cross-reference GLADE galaxies by their “PGC ID” with the Principal Galaxy Catalog (PGC) and use the corresponding corrected radial velocities in the heliocentric frame (Kourkchi & Tully 2017). We then correct these heliocentric velocities to the CMB frame using NASA/IPAC Extragalactic Database (NED) with parameters $l_{\text{apex}} = 264.14^\circ$, $b_{\text{apex}} = +48.26^\circ$,

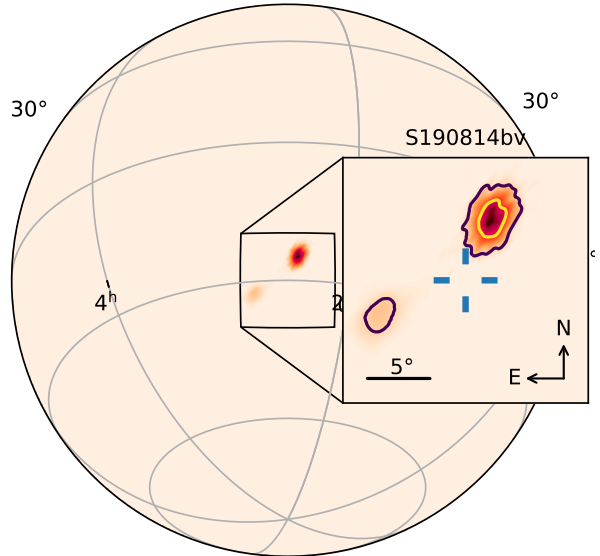


Figure 1. Globe projected skymap for GW190814 (S190814bv) using the `ligo-skymap-plot` module. The inset shows a close-up view centered on (RA = 1^{hr}, Dec = −30°; blue tick marks). Dark purple and yellow contours represent the 90% (23 deg²) and 50% (5 deg²) credible regions, respectively.

and $v_{\text{apex}} = 371.0 \text{ km s}^{-1}$ (Fixsen et al. 1996). We define the z_{rad} and z_{CMB} parameters as the radial group velocity and CMB reference frame corrections, respectively. Finally, we assign a 200 km s^{-1} Gaussian uncertainty to the velocity (cz) for each galaxy.

For our purposes, we only extract the right ascension (degrees), declination (degrees), redshift, apparent B magnitude, and absolute B magnitude (RA, Dec, z , B , B_{abs} , respectively) from the raw catalog and build the pickle⁴-formatted dictionary that `gwcosmo` requires. Note that `gwcosmo` expects the RA and Dec to be in radians. We use the provided B -band magnitude in our galaxy-weighting procedures.

2.3. Skymap Localization

During O2 and O3, LIGO-Virgo released public alerts accompanied by an allsky HEALPix localization skymap in a FITS file format for each GW event. The skymap FITS includes the sky position, probability, and distance for each pixel. The original 90% region for GW170817 (28 deg²) was improved to 16 deg² using the LALInference pipeline (Veitch et al. 2015). For our analysis, we adopt the updated skymap.⁵

⁴ <https://docs.python.org/3/library/pickle.html>.

⁵ We use the updated GW170817 skymap named `figure_3.tar.gz`.

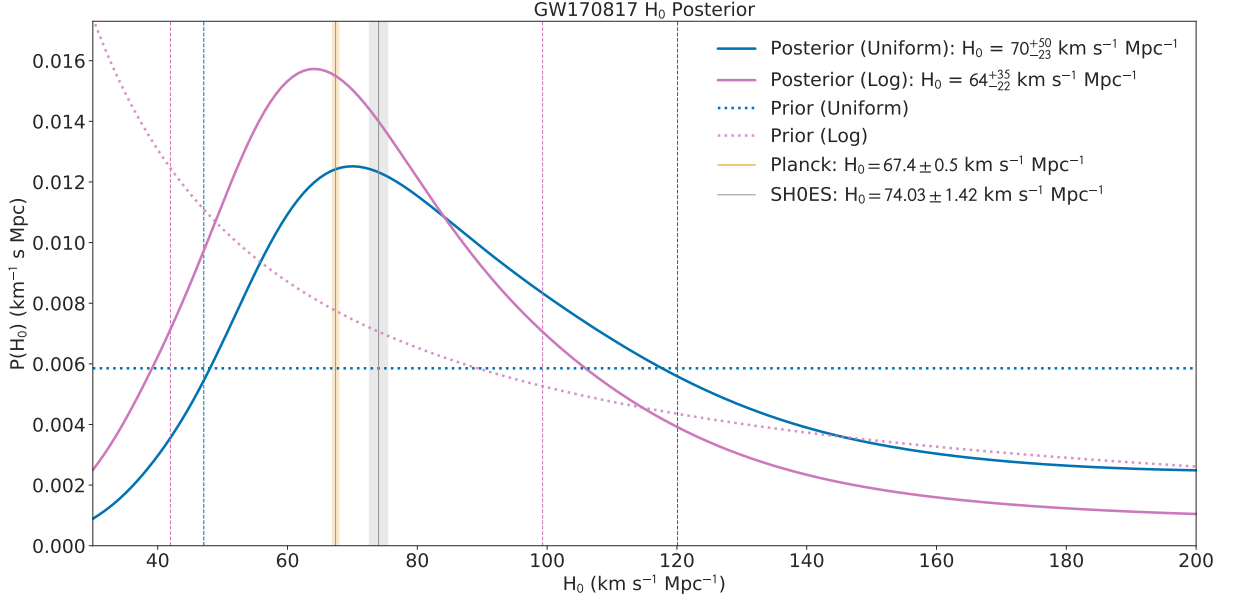


Figure 2. H_0 posterior for GW170817 (no-counterpart) assuming a flat log (purple) and uniform (blue) prior on H_0 along the interval $[30, 200] \text{ km s}^{-1} \text{ Mpc}^{-1}$. Here, we adopt the Gaussian BNS mass distribution with $\mu = 1.35 M_\odot$, $\sigma = 0.15 M_\odot$. The B -band luminosity threshold is $L_B \geq 0.001 L_B^*$. All galaxies have equal luminosity weights and negligible redshift uncertainties. We include the most recent *Planck* (orange vertical line) and SH0ES (grey vertical line) measurements and their corresponding 1σ uncertainties (shaded regions).

Table 1. Input parameters and corresponding H_0 posterior results for GW190814

Row	Luminosity Threshold	Redshift Correction	Galaxy Weighting	H_0 Posterior
Name	B band	Type	Bool	68% ($\text{km s}^{-1} \text{ Mpc}^{-1}$)
A	$\geq 0.001 L_B^*$	$z_{\text{rad}}, z_{\text{CMB}}$	False	$67^{+41.0}_{-26.0}$
B	$\geq 0.01 L_B^*$	$z_{\text{rad}}, z_{\text{CMB}}$	False	$68^{+39.0}_{-28.0}$
C	$\geq 0.001 L_B^*$	$z_{\text{rad}}, z_{\text{CMB}}$	True	$66^{+55.0}_{-12.0}$
D	$\geq 0.25 L_B^*$	$z_{\text{rad}}, z_{\text{CMB}}$	False	$69^{+39.0}_{-28.0}$
E	$\geq 0.626 L_B^*$	$z_{\text{rad}}, z_{\text{CMB}}$	False	$71^{+34.0}_{-30.0}$
F	$\geq 0.001 L_B^*$	None	False	$68^{+40.0}_{-27.0}$
G	$\geq 0.01 L_B^*$	None	False	$68^{+40.0}_{-27.0}$
H	$\geq 0.001 L_B^*$	None	True	$66^{+52.0}_{-15.0}$
I	$\geq 0.25 L_B^*$	None	False	$70^{+48.0}_{-19.0}$
J	$\geq 0.626 L_B^*$	None	False	$72^{+42.0}_{-23.0}$

NOTE—The z_{rad} and z_{CMB} labels signify that we applied the radial group velocity and CMB reference frame corrections discussed in Section 2.2. The following parameters are constant for each measurement. H_0 prior, Uniform $[40, 140] \text{ (km s}^{-1} \text{ Mpc}^{-1})$; PSD, O3; mass distribution, NSBH-Uniform; completeness, False.

For GW190814, we use the updated skymap from the GraceDB database, localizing the source to 23 deg^2 and 5 deg^2 in the 90% and 50% confidence regions, respectively⁶.

⁶ The publicly available updated S190814bv skymap LALInference.v1.fits.gz is available at [GraceDb](https://gracedb.org).

The marginalized distance posterior found in the skymap is a symmetric Gaussian fit to the full, potentially asymmetric posterior sample. According to Fishbach et al. (2019), this assumption has the effect of moving the peak of the H_0 posterior by as much as 9% compared to using a full posterior sample. For our calculations, Equation A5 of the Appendix only includes galaxies in the 99.9% region (assigning weight

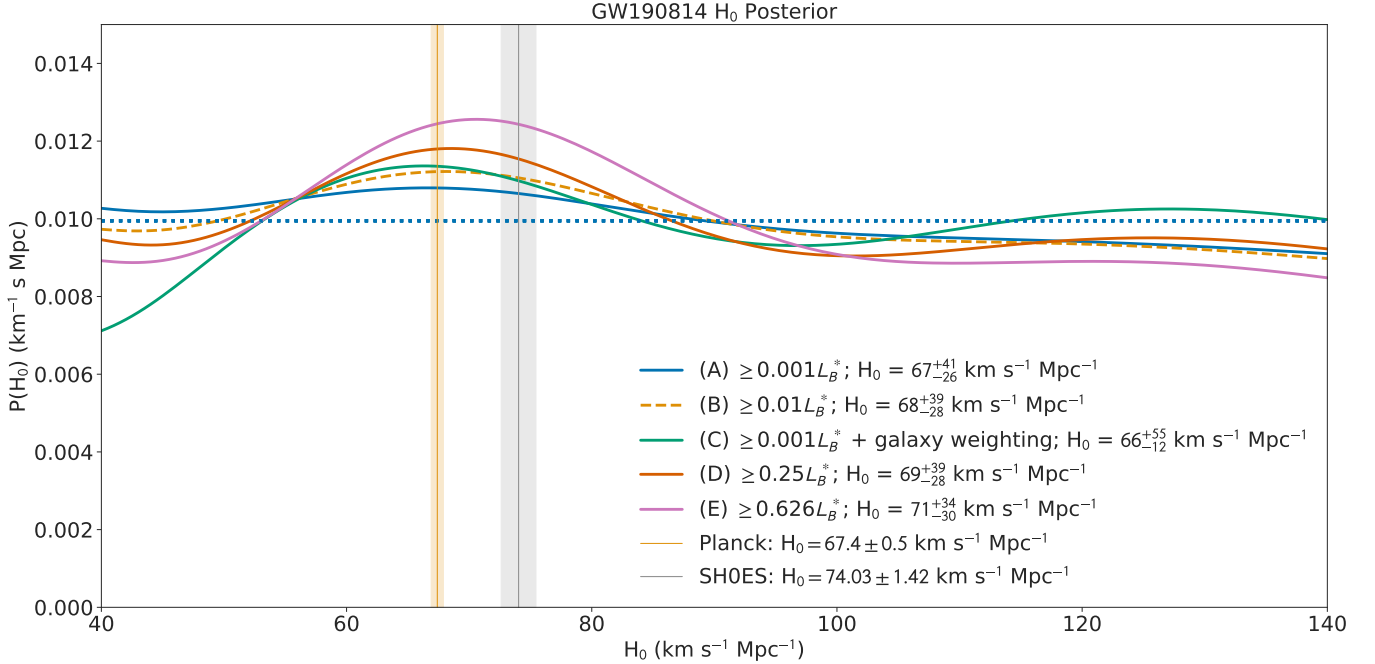


Figure 3. Combined H_0 posterior for GW190814 assuming a uniform (dotted blue) H_0 prior along the interval $[40, 140] \text{ km s}^{-1} \text{ Mpc}^{-1}$. Lettering in the legend corresponds to the rows in Table 1. We illustrate the incremental appearance of structure in the posterior as the luminosity threshold is increased. For A (solid blue), B (dotted orange), D (solid red orange), and E (pink), we set a luminosity threshold of $0.001 L_B^*$, $0.01 L_B^*$, $0.25 L_B^*$, and $0.626 L_B^*$, respectively. C (solid green) shows the posterior when the luminosity threshold is $0.001 L_B^*$ and *galaxy weighting* is set to “True.” We include the most recent *Planck* (orange vertical line) and SH0ES (gray vertical line) measurements and their corresponding 1σ uncertainties (shaded regions).

= 1 to each if equal weights) and assigns a weight of 0 for those outside of the localization region.

3. RESULTS

We split our analysis into two parts. First, we summarize our results for GW170817 and compare our H_0 inference to previous works using this statistical method (Gray et al. 2019; Fishbach et al. 2019; Abbott et al. 2019c). We also explore possible systematic differences and assumptions that may carry into our H_0 calculation for GW190814. We then repeat the procedure over the parameter space introduced in Section 2 for GW190814. All H_0 measurements assume the 68.3% highest density posterior interval. We choose the H_0 prior range as $[30, 200]$ or $[40, 140] \text{ km s}^{-1} \text{ Mpc}^{-1}$ for ease of comparison to other works. Finally, we repeat the calculation using the full posterior samples released by the LVC on June 25, 2020.

We note that after submission and initial review of this paper, the Dark Energy Survey (DES) Collaboration posted a paper (Palmese et al. 2020) in which a similar analysis of GW190814 is presented, but they did not include posterior samples.

3.1. Statistical Method

Since the GLADE catalog is 100% complete up to $z = 0.03$ for galaxies that are above $0.25 L_B^*$, and we consider

galaxies well above this redshift threshold and down to $0.001 L_B^*$ ($M_B = -12.96 \text{ mag}$), we set the completeness parameter to “False” in our final calculation unless stated otherwise. We consider a flat log and uniform prior on H_0 on the intervals $[30, 200]$ and $[40, 140] \text{ km s}^{-1} \text{ Mpc}^{-1}$. We use the BNS-Gaussian mass distribution centered on $\mu = 1.35 M_\odot$ and a standard deviation of $\sigma = 0.15 M_\odot$. Galaxies up to $z \approx 0.5$ ($z_{\text{max}} = 0.5$) are allowed, with equal luminosity weights assigned. A 200 km s^{-1} Gaussian uncertainty is applied to the velocity (cz) of each galaxy. 2662 galaxies fall into the 99% skymap localization corresponding to 34 deg^2 . We employ a constant rate evolution term discussed in Section 2.1. The resulting H_0 posterior is illustrated in Figure 2.

Given a uniform H_0 prior along the intervals $[30, 200]$ and $[40, 140] \text{ km s}^{-1} \text{ Mpc}^{-1}$, we infer a Hubble constant $70_{-23.0}^{+50.0} \text{ km s}^{-1} \text{ Mpc}^{-1}$ and $70_{-18.0}^{+35.0} \text{ km s}^{-1} \text{ Mpc}^{-1}$, respectively. Even when accounting for a luminosity cut $\geq 0.626 L_B^*$ yielding $H_0 = 73_{-17.0}^{+36.0}$, our peak is less pronounced and is shifted compared to the $H_0 \geq 74 \text{ km s}^{-1} \text{ Mpc}^{-1}$ obtained by Fishbach et al. (2019). This discrepancy may be caused by differences in both our chosen subset of the GLADE galaxy catalog and our velocity corrections. As a qualitative test, we also calculate H_0 without the radial group velocity and CMB reference frame corrections,

yielding $67_{-19.0}^{+37.0}$ km s⁻¹ Mpc⁻¹ for a uniform H_0 prior interval, [40, 140] km s⁻¹ Mpc⁻¹. Given the sensitivity of the posterior to the injected catalog, we expect a slight deviation if the catalog is handled differently. These systematic differences will carry over into our calculation for the NS-BH merger.

For GW190814, we assume the same B -band Schechter parameters chosen for the GW170817 calculations. Here, we focus only on the [40, 140] km s⁻¹ Mpc⁻¹ prior range on H_0 . We show our results in Table 1 and illustrate the H_0 posterior in Figure 3, where we plot five realizations for different luminosity considerations. We apply a maximum redshift limit $z_{\max} = 0.5$ and assume the NSBH-uniform mass distribution. 64,735 galaxies are obtained in the 99% localization region. We repeat the calculation for GW190814 to obtain $H_0 = 67_{-26.0}^{+41.0}$ km s⁻¹ Mpc⁻¹ and $H_0 = 71_{-30.0}^{+34.0}$ km s⁻¹ Mpc⁻¹ for $L_B \geq 0.001 L_B^*$ and $L_B \geq 0.626 L_B^*$, respectively. Our tested parameter space is detailed in Table 1. According to Figure 3, the posterior peak is more pronounced for stricter luminosity cuts. The peak of our H_0 posterior shifts by $\sim 6\%$ over the range of luminosity cuts, which is in agreement with Fishbach et al. (2019). The GW190814 posterior appears significantly flatter compared to GW170817. Given that the GW190814 localization covered a larger volume and included more than ten times as many galaxies as GW170817, we expect the GW190814 posterior to be washed out. The bump in the $H_0 = 100\text{--}140$ km s⁻¹ Mpc⁻¹ range is enhanced when *galaxy weighting* is set to “True”; it may be an artifact of enhanced GLADE catalog features similar to Figure 2 of Abbott et al. (2019c).

We then combine the posteriors for GW170817 with S190814 using the *gwcosmo_combined_posterior* script, yielding $H_0 = 70_{-18.0}^{+29.0}$ km s⁻¹ Mpc⁻¹ as shown in Figure 4. Although the peak is centered between the *Planck* and SH0ES results, we caution that the value is subject to systematics arising from luminosity cuts or weighting. For example, our combined posterior used a luminosity threshold of $0.626 L_B^*$ for GW190814, whereas taking the luminosity down to $0.001 L_B$ would produce a peak at $H_0 \leq 70$ km s⁻¹ Mpc⁻¹. The combined posterior demonstrates the ability to further constrain the Hubble constant with multiple GW sources.

Systematic biases in the joint posterior due to varying population parameters of astrophysical sources are expected to be smaller than the statistical uncertainties due to contributions from the galaxy catalog given a high probability that the host galaxy is in the catalog. GW190814 has a median source redshift of $z_{\text{event}} = 0.053$ using the combined waveform model from Abbott et al. (2020), corresponding to $p(G|z_{\text{event}}, D_w) > 0.6$ (or “high in-catalog probability”) with the GLADE catalog according to Figure 1 of Abbott et al. (2019c). Therefore, we take the contributions from the

galaxy catalog to be the dominant source of uncertainties for GW190814.

3.2. Using the Posterior Samples

In light of the LVC data release for GW190814 on June 25, 2020, we apply the full posterior sample to our H_0 calculation (Abbott et al. 2020). We now account for biases introduced when a Gaussian approximation to the distance posterior is used via the 3D skymap. For GW170817, we use the low-spin PhenomPNRT posterior sample⁷. For GW190814, we use a combined posterior sample consisting of the SEOB-NRv4PHM (EOBNR PHM; Babak et al. 2017; Ossokine et al. 2020) and IMRPhenomPv3HM (Phenom PHM; Khan et al. 2019, 2020) Waveform Models.⁸ In Figure 6, we compare the differences in the GW190814 H_0 posterior with and without the use of posterior samples.

Following the reasoning of Fishbach et al. (2019), the use of a full posterior sample (accounting for masses and spins) as opposed to a Gaussian approximation to the distance posterior can have the effect of shifting the H_0 posterior peak. In our case, we observe a notable shift for both sets of parameters, favoring a higher value for the Hubble constant when using posterior samples. In Figure 6, we show the combined H_0 posterior following the same procedure used to produce Figure 4, but now with posterior samples for both GW170817 and GW190814. We obtain $H_0 = 67_{-15.0}^{+36.0}$ km s⁻¹ Mpc⁻¹ (GW170817; $L_B \geq 0.001 L_B^*$), $H_0 = 75_{-20.0}^{+45.0}$ km s⁻¹ Mpc⁻¹ (GW190814; $L_B \geq 0.001 L_B^*$), and $H_0 = 77_{-25.0}^{+39.0}$ km s⁻¹ Mpc⁻¹ (GW190814; $L_B \geq 0.626 L_B^*$), in agreement with the results of Abbott et al. (2020). Our combined H_0 calculation with posterior samples yields $H_0 = 69_{-14.0}^{+29.0}$ km s⁻¹ Mpc⁻¹. Here, we observe a slight improvement to the uncertainty in the combined H_0 inference, owing to the additional information gained when using posterior samples.

4. CONCLUSIONS

We demonstrated the statistical catalog method to infer the value of H_0 for GW sources without an optical counterpart. Previous measurements have been made for GW events in O1 and O2, most notably with GW170817. Our baseline test served as a calibration against the result of Fishbach et al. (2019) to identify systematic differences that may affect our H_0 measurement for NS-BH merger GW190814. Using a uniform H_0 prior [40,140] km s⁻¹ Mpc⁻¹ with a luminosity threshold of $0.001 L_B^*$ for both GW170817 and

⁷ The posterior sample file can be found at LIGO-P1800061-v11.

⁸ Relevant files can be accessed at Gravitational Wave Open Science Center.

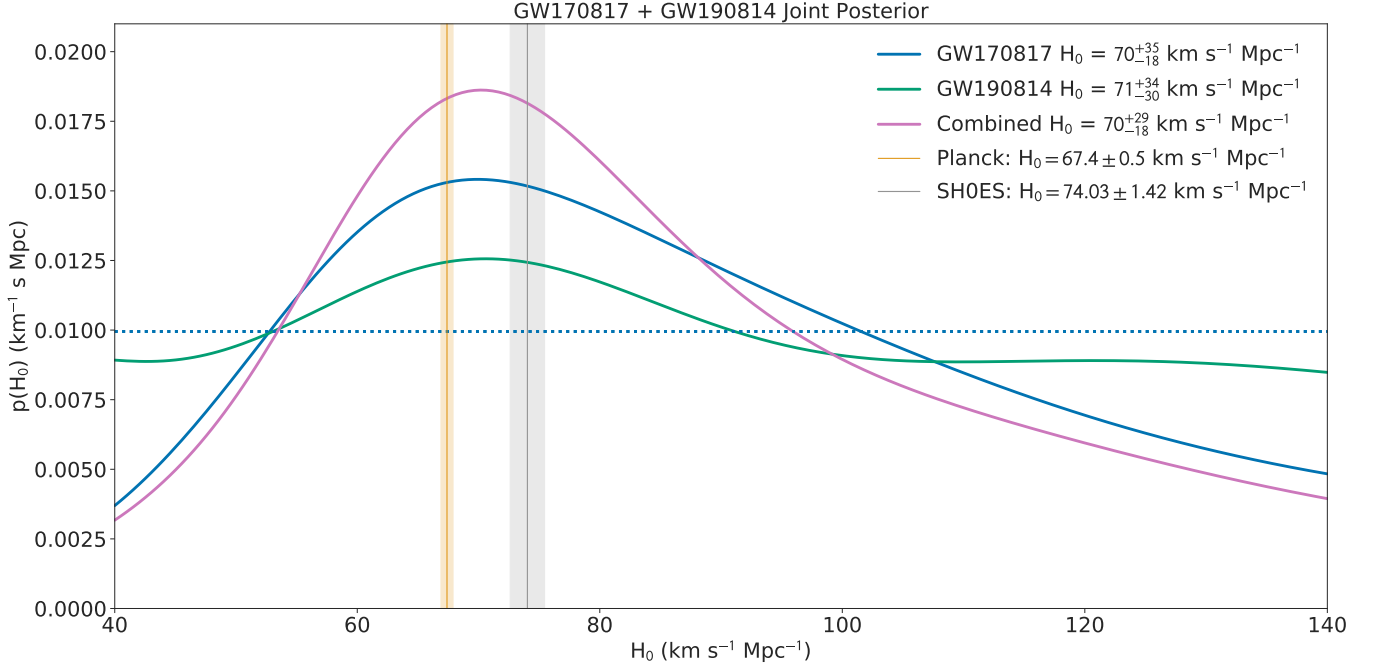


Figure 4. Combined H_0 posterior for GW170817 and GW190814 assuming uniform (dotted blue) H_0 prior along the interval $[40, 140] \text{ km s}^{-1} \text{ Mpc}^{-1}$. For GW190814, we use the parameters in Row E from Table 1. We include the most recent *Planck* (orange vertical line) and SH0ES (gray vertical line) measurements and their corresponding 1σ uncertainties (shaded regions).

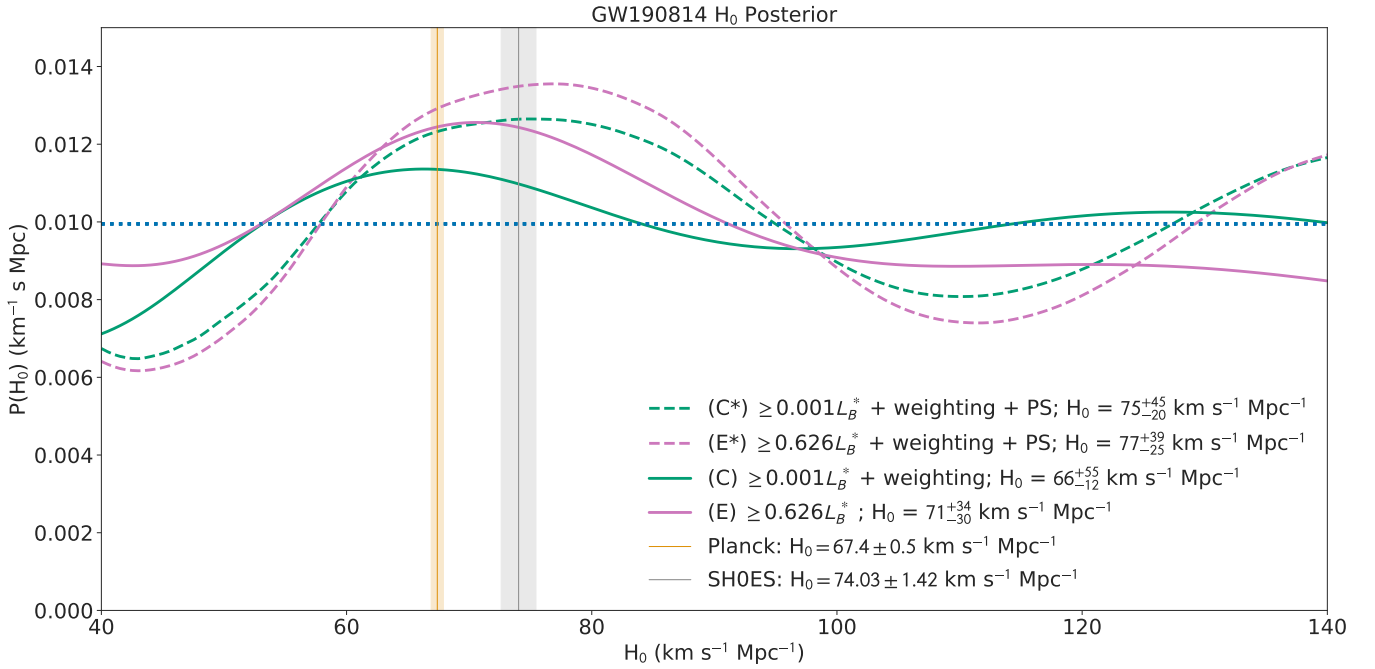


Figure 5. H_0 posterior for GW190814 assuming a uniform (dotted blue) H_0 prior along the interval $[40, 140] \text{ km s}^{-1} \text{ Mpc}^{-1}$. Lettering in the legend corresponds to the rows in Table 1. We illustrate the difference between using posterior samples (a combined SEOBNRv4PHM and IMRPhenomPv3HM waveform model) and using a Gaussian approximation to the distance posterior from the 3D skymap. The C (solid green) and E (solid pink) curves are identical to those in Figure 4. We label C* (dashed green) and E* (dashed purple) to indicate when posterior samples are used. We include the most recent *Planck* (orange vertical line) and SH0ES (gray vertical line) measurements and their corresponding 1σ uncertainties (shaded regions).

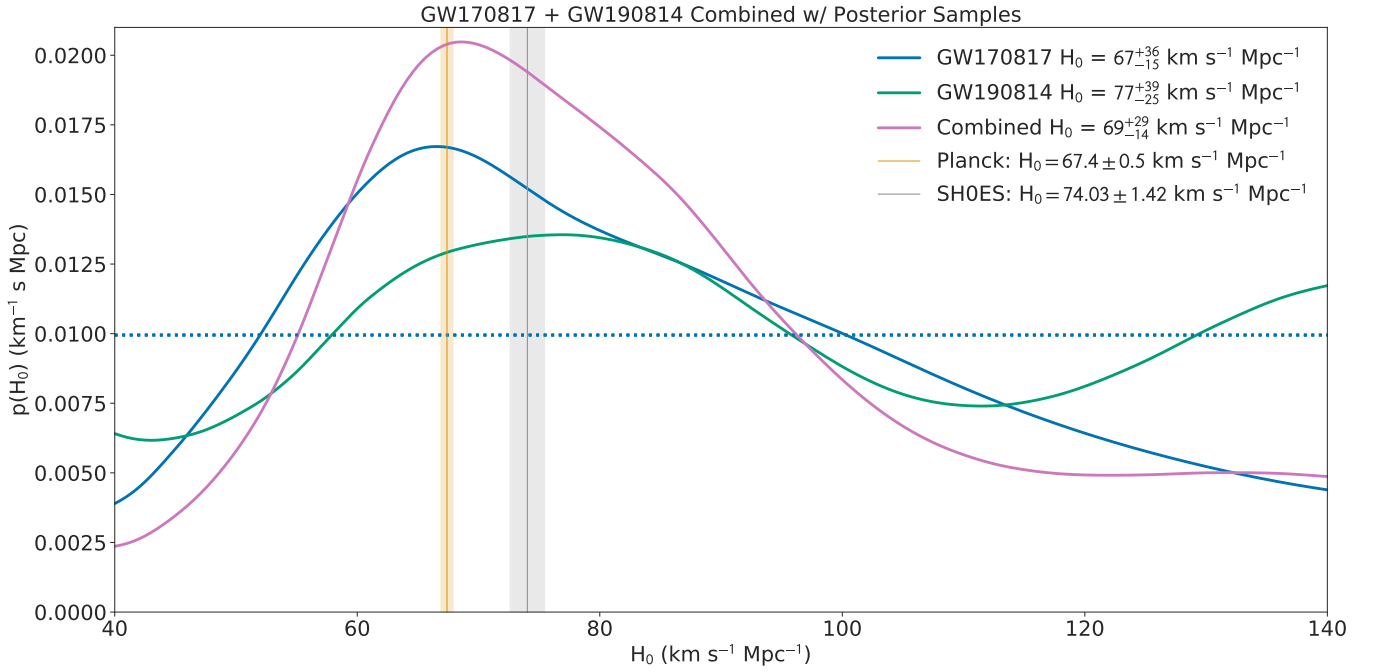


Figure 6. Combined H_0 posterior for GW170817 and GW190814 assuming uniform (dotted blue) H_0 prior along the interval $[40, 140] \text{ km s}^{-1} \text{ Mpc}^{-1}$. The GW170817 posterior (solid blue line) is now calculated using a low spin PhenomPNRT posterior sample. For GW190814, we use the parameters in Row E from Table 1 together with a SEOBNRv4PHM + IMRPhenomPv3HM posterior sample (labeled E* in Figure 5). We include the most recent *Planck* (orange vertical line) and SH0ES (gray vertical line) measurements and their corresponding 1σ uncertainties (shaded regions).

GW190814, we infer $H_0 = 70_{-18.0}^{+35.0} \text{ km s}^{-1} \text{ Mpc}^{-1}$ and $67_{-26.0}^{+41.0} \text{ km s}^{-1} \text{ Mpc}^{-1}$, respectively. We then increased the luminosity threshold up to $L_B \geq 0.626 L_B^*$ and obtain $H_0 = 71_{-30.0}^{+34.0} \text{ km s}^{-1} \text{ Mpc}^{-1}$ for GW190814. This tighter value is used in combination with the GW170817 posterior to achieve a final value of $H_0 = 70_{-18.0}^{+29.0} \text{ km s}^{-1} \text{ Mpc}^{-1}$. We repeat the individual and joint inferences using the low-spin PhenomPNRT and combined (SEOBNRv4PHM + IMRPhenomPv3HM) posterior samples for GW170817 and GW190814, respectively. We achieve a tighter constraint for the joint measurement with $H_0 = 69_{-14.0}^{+29.0} \text{ km s}^{-1} \text{ Mpc}^{-1}$ when using posterior samples. Several sources of systemat-

ics were identified, including the injected catalog, luminosity weighting, and luminosity thresholds.

The motivation for this method follows the expectation of having significantly more GW-only mergers (dark sirens) than mergers with optical counterparts, providing a valuable test for H_0 inferences using the electromagnetic counterpart. As we head into the next generation of gravitational-wave detectors, the standard-siren method will improve the constraints on the Hubble constant. This new independent method may potentially resolve the Hubble tension problem or compel us to reevaluate our cosmological models, specifically Λ -CDM.

APPENDIX

The Statistical Method

Here, we summarize the statistical method adopted from [Chen et al. \(2018\)](#), [Gray et al. \(2019\)](#), and [Abbott et al. \(2019c\)](#). For relevant formalism, also see [Mandel et al. \(2019\)](#), [Thrane & Talbot \(2019\)](#), and [Vitale \(2020\)](#).

The posterior probability on H_0 from N gravitational-wave (GW) events can be computed as

$$\begin{aligned} p(H_0|x_{\text{GW}}, D_{\text{GW}}) &= \frac{p(H_0)p(N|H_0) \prod_i^N p(x_{\text{GW}i}|D_{\text{GW}i}, H_0)}{p(x_{\text{GW}}|D_{\text{GW}})} \\ &\propto p(H_0) \prod_i^N p(x_{\text{GW}i}|D_{\text{GW}i}, H_0), \end{aligned} \quad (\text{A1})$$

where x_{GW} is the set of GW data and D_{GW} indicates that the detection was made in the form of a GW. Here, $p(H_0)$ is the prior on H_0 that we took to be either uniform or flat log over an interval [a,b]. $p(N|H_0)$ is the likelihood of detecting N events given a value for H_0 . Using the same prior on the astrophysical rate of events as in [Abbott et al. \(2019c\)](#), we drop the dependence of this term on H_0 .

For an individual gravitational-wave event, the likelihood can be written as

$$\begin{aligned} p(x_{\text{GW}}|D_{\text{GW}}, H_0) &= \frac{p(D_{\text{GW}}|x_{\text{GW}}, H_0)p(x_{\text{GW}}|H_0)}{p(D_{\text{GW}}|H_0)}, \\ &= \frac{p(x_{\text{GW}}|H_0)}{p(D_{\text{GW}}|H_0)}, \end{aligned} \quad (\text{A2})$$

The normalization factor $p(D_{\text{GW}}|H_0)$ in the denominator of Eq. A2 can be evaluated with the integral

$$\begin{aligned} p(D_{\text{GW}}|H_0) &= \int p(D_{\text{GW}}|x_{\text{GW}}, H_0)p(x_{\text{GW}}|H_0)dx_{\text{GW}} \\ &= \int_{\rho > \rho_{\text{th}}}^{\infty} p(x_{\text{GW}}|H_0)dx_{\text{GW}}, \end{aligned} \quad (\text{A3})$$

where ρ_{th} is the signal-to-noise ratio (SNR) threshold below which $p(D_{\text{GW}}|H_0) = 0$. In our calculations we assume $\rho_{\text{th}} = 8$, the default in gwcosmo. Calculating the event detectability, $p(D_{\text{GW}}|H_0)$, involves marginalizing over masses, inclination, polarization, and sky location. Gwcosmo (detection_probability.py) uses a Monte-Carlo integration to marginalize over many GW events. The source masses are drawn from the prior mass distribution $p(m_1, m_2)$, defined in Section 2.1. The source masses are converted to observed masses when setting *Basic pdet* to “False”. Treatment of mass distributions is described in more detail in

Appendix 5 of Gray et al. (2019).⁹

In our case, we use the galaxy-catalog method, in which the likelihood function $p(x_{\text{GW}}|D_{\text{GW}}, H_0)$ can be expanded as

$$\begin{aligned} p(x_{\text{GW}}|D_{\text{GW}}, H_0) &= \sum_{g=G, \bar{G}} p(x_{\text{GW}}, g|D_{\text{GW}}, H_0) \\ &= \sum_{g=G, \bar{G}} p(x_{\text{GW}}|g, D_{\text{GW}}, H_0)p(g|D_{\text{GW}}, H_0) \\ &= p(x_{\text{GW}}|G, D_{\text{GW}}, H_0)p(G|D_{\text{GW}}, H_0) + p(x_{\text{GW}}|\bar{G}, D_{\text{GW}}, H_0)p(\bar{G}|D_{\text{GW}}, H_0). \end{aligned} \quad (\text{A4})$$

with G and \bar{G} denoting the cases where the host is in the catalog and where it is not, respectively.

The likelihood *when* the host galaxy is in the catalog, $p(x_{\text{GW}}|G, D_{\text{GW}}, H_0)$, can be written as

$$p(x_{\text{GW}}|G, D_{\text{GW}}, H_0) = \frac{\sum_{i=1}^{N_{\text{gal}}} \int p(x_{\text{GW}}|z_i, \Omega_i, H_0)p(s|M(z_i, m_i, H_0))p(z_i)dz_i}{\sum_{i=1}^{N_{\text{gal}}} \int p(D_{\text{GW}}|z_i, \Omega_i, H_0)p(s|M(z_i, m_i, H_0))p(z_i)dz_i}, \quad (\text{A5})$$

where N_{gal} is the number of galaxies considered in the catalog, $\Omega(\alpha, \delta)$ is the sky position angle, z_i is the redshift of galaxy, s indicates that a GW has been emitted (distinct from detected), and m_i and M are respectively the apparent and absolute magnitude of the galaxy.

Luminosity weighting:

$$p(s|M, H_0) \propto \begin{cases} L(M(H_0)) & \text{galaxy (luminosity) weighting = True} \\ \text{const.} & \text{galaxy weighting = False.} \end{cases} \quad (\text{A6})$$

Redshift evolution rate:

$$p(s|z) \propto \begin{cases} (1+z)^\lambda & \text{if rate evolves with redshift} \\ \text{const.} & \text{if rate is constant with redshift,} \end{cases} \quad (\text{A7})$$

where λ is the rate evolution parameter, whose default value is 3.0 in gwcosmo. However, we hold the rate constant throughout all calculations. We define $V_c(z)$ as the co-moving volume contained within a redshift z .

Redshift prior:

$$p(z) \propto \frac{1}{1+z} \frac{V_c(z)}{dz}, \text{ if merger rate density = const.} \quad (\text{A8})$$

The likelihood when the host galaxy is not in the catalog is defined as

$$p(x_{\text{GW}}|\bar{G}, D_{\text{GW}}, H_0) = \frac{\int \int \int_0^\infty \int_{z(M, m_{\text{th}}, H_0)}^\infty p(x_{\text{GW}}|z, \Omega, H_0)p(z)p(\Omega)p(s|M, H_0)p(M|H_0)dzd\Omega dM}{\int \int \int_0^\infty \int_{z(M, m_{\text{th}}, H_0)}^\infty p(D_{\text{GW}}|z, \Omega, H_0)p(z)p(\Omega)p(s|M, H_0)p(M|H_0)dzd\Omega dM}. \quad (\text{A9})$$

$$p(G|D_{\text{GW}}, H_0) = \frac{\int \int \int_0^{z(M, m_{\text{th}}, H_0)} p(D_{\text{GW}}|z, \Omega, H_0)p(s|z)p(z)p(\Omega)p(s|M, H_0)p(M|H_0)dzd\Omega dM}{\int \int \int_0^\infty p(D_{\text{GW}}|z, \Omega, H_0)p(s|z)p(z)p(\Omega)p(s|M, H_0)p(M|H_0)dzd\Omega dM}, \quad (\text{A10})$$

$$p(\bar{G}|D_{\text{GW}}, H_0) = 1 - p(G|D_{\text{GW}}, H_0). \quad (\text{A11})$$

⁹ The calculation of Eq. (A3) has been a widely explored topic in the literature. Systematic biases can arise when this quantity does not fully account for all of the parameters on which the gravitational-wave signal is dependent. We emphasize that these effects are insignificant compared to the statistical contribution from the galaxy catalog, as discussed in Section 3.1.

Equations A10 and A11 are the probabilities that the host *is* and *is not* in the galaxy catalog, respectively.

The prior on the GW host-galaxy sky location, $p(\Omega)$, is taken to be uniform across the sky.

The prior on the absolute magnitude, $p(M|H_0)$, is taken to be proportional to the Schechter (1976) luminosity function, the parameters for which are defined in Section 2.2. Here, m_{th} is the apparent magnitude threshold of the flux-limited galaxy catalog.

A complete description of the mathematics in gwcosmo is given in the Appendix of Gray et al. (2019).

ACKNOWLEDGMENTS

We thank Benjamin Stahl and Keto Zhang (U.C. Berkeley) for helpful advice on writing this paper, as well as the anonymous referee whose suggestions improved its quality. Ignacio Magaña Hernandez (U.W. Milwaukee) discussed gwcosmo with us. We are also grateful to the lscsoft team for their efforts in providing public access to the gwcosmo code. Generous financial support for this work was provided by Steven Nelson, the Christopher R. Redlich Fund, and the Miller Institute for Basic Research in Science (U.C. Berkeley).

REFERENCES

- Abbott, B., Abbott, R., Abbott, T., et al. 2017a, *Physical Review Letters*, 119, 161101. <https://link.aps.org/doi/10.1103/PhysRevLett.119.161101>
- Abbott, B. P., Abbott, R., Abbott, T. D., et al. 2017b, *Nature*, 551, 85. <http://arxiv.org/abs/1710.05835>
- . 2019a, *Physical Review X*, 9, 011001. <http://arxiv.org/abs/1805.11579>
- . 2019b, *Physical Review Letters*, 123, 011102. <http://arxiv.org/abs/1811.00364>
- . 2019c, arXiv:1908.06060 [astro-ph, physics:gr-qc]. <http://arxiv.org/abs/1908.06060>
- Abbott, R., Abbott, T. D., Abraham, S., et al. 2020, *The Astrophysical Journal*, 896, L44. <https://doi.org/10.3847/2F2041-8213%2F20200411>
- Abbott, T. M. C., Abdalla, F. B., Allam, S., et al. 2018, *ApJ Supplement Series*, 239, 18. <http://arxiv.org/abs/1801.03181>
- Annala, E., Gorda, T., Kurkela, A., & Vuorinen, A. 2018, *Physical Review Letters*, 120, 172703. <http://arxiv.org/abs/1711.02644>
- Arcavi, I., McCully, C., Hosseinzadeh, G., et al. 2017, *ApJ*, 848, L33. <https://doi.org/10.3847/2F2041-8213%2F20170411>
- Babak, S., Taracchini, A., & Buonanno, A. 2017, *Physical Review D*, 95, 024010. <http://adsabs.harvard.edu/abs/2017PhRvD..95b4010B>
- Baibhav, V., Berti, E., Gerosa, D., et al. 2019, *Physical Review D*, 100, 064060. <http://arxiv.org/abs/1906.04197>
- Barbieri, C., Salafia, O. S., Perego, A., Colpi, M., & Ghirlanda, G. 2020, *European Physical Journal A*, 56, 8. <http://adsabs.harvard.edu/abs/2020EPJA...56....8B>
- Carrick, J., Turnbull, S. J., Lavaux, G., & Hudson, M. J. 2015, *MNRAS*, 450, 317. <http://arxiv.org/abs/1504.04627>
- Chen, H.-Y., Fishbach, M., & Holz, D. E. 2018, *Nature*, 562, 545. <http://arxiv.org/abs/1712.06531>
- Chen, X., Li, S., & Cao, Z. 2019, *MNRAS: Letters*, 485, L141. <http://arxiv.org/abs/1703.10543>
- Coulter, D. A., Foley, R. J., Kilpatrick, C. D., et al. 2017, *Science*, 358, 1556. <http://arxiv.org/abs/1710.05452>
- Cuceu, A., Farr, J., Lemos, P., & Font-Ribera, A. 2019, *Journal of Cosmology and Astroparticle Physics*, 2019, 044. <http://arxiv.org/abs/1906.11628>
- Del Pozzo, W. 2012, *Physical Review D*, 86, 043011. <http://adsabs.harvard.edu/abs/2012PhRvD..86d3011D>
- Dlya, G., Galgoczy, G., Dobos, L., et al. 2018, *MNRAS*, 479, 2374. <http://arxiv.org/abs/1804.05709>
- Feeney, S. M., Peiris, H. V., Williamson, A. R., et al. 2019, *Physical Review Letters*, 122, 061105. <http://arxiv.org/abs/1802.03404>
- Fishbach, M., Gray, R., Hernandez, I. M., et al. 2019, *ApJ*, 871, L13. <http://arxiv.org/abs/1807.05667>
- Fixsen, D. J., Cheng, E. S., Gales, J. M., et al. 1996, *ApJ*, 473, 576. <http://adsabs.harvard.edu/abs/1996ApJ...473..576F>
- Fong, W., & Berger, E. 2013, *ApJ*, 776, 18. <https://doi.org/10.1088/2F0004-637x%2F776%2F1%2F18>
- Foucart, F., Duez, M. D., Kidder, L. E., et al. 2019, *Physical Review D*, 99, 103025. <http://arxiv.org/abs/1903.09166>
- Foucart, F., Hinderer, T., & Nisanke, S. 2018, *Physical Review D*, 98, 081501. <http://arxiv.org/abs/1807.00011>
- Gehrels, N., Cannizzo, J. K., Kanner, J., et al. 2016, *ApJ*, 820, 136. <https://iopscience.iop.org/article/10.3847/0004-637X/820/2/136>
- Goldstein, A., Veres, P., Burns, E., et al. 2017, *ApJ*, 848, L14. <https://doi.org/10.3847/2F2041-8213%2F20170411>
- Gray, R., Hernandez, I. M., Qi, H., et al. 2019, arXiv:1908.06050 [astro-ph, physics:gr-qc]. <http://arxiv.org/abs/1908.06050>
- Hatt, D., Freedman, W. L., Madore, B. F., et al. 2018, *ApJ*, 866, 145. <http://arxiv.org/abs/1809.01741>
- Hinshaw, G., Weiland, J. L., Hill, R. S., et al. 2009, 46
- Holz, D. E., & Hughes, S. A. 2005, *The Astrophysical Journal*, 629, 15. <http://arxiv.org/abs/astro-ph/0504616>
- Huang, C. D., Riess, A. G., Yuan, W., et al. 2020, *ApJ*, 889, 5. <http://arxiv.org/abs/1908.10883>
- Jang, I. S., & Lee, M. G. 2017, *ApJ*, 836, 74. <https://doi.org/10.3847/2F1538-4357%2F836%2F1%2F74>
- KAGRA Collaboration, LIGO Scientific Collaboration, and Virgo Collaboration, Abbott, B. P., Abbott, R., et al. 2018, *Living Reviews in Relativity*, 21, 3. <http://link.springer.com/10.1007/s41114-018-0012-9>
- Kasen, D., Metzger, B., Barnes, J., Quataert, E., & Ramirez-Ruiz, E. 2017, *Nature*, 551, 80. <http://arxiv.org/abs/1710.05463>
- Khan, S., Chatziioannou, K., Hannam, M., & Ohme, F. 2019, *Physical Review D*, 100, 024059. <http://adsabs.harvard.edu/abs/2019PhRvD.100b4059K>
- Khan, S., Ohme, F., Chatziioannou, K., & Hannam, M. 2020, *Physical Review D*, 101, 024056. <http://adsabs.harvard.edu/abs/2020PhRvD.101b4056K>
- Kiziltan, B., Kottas, A., & Thorsett, S. E. 2010, arXiv:1011.4291 [astro-ph, stat]. <http://arxiv.org/abs/1011.4291>
- Kourkchi, E., & Tully, R. B. 2017, *ApJ*, 843, 16. <http://arxiv.org/abs/1705.08068>
- LIGO Scientific Collaboration, & Virgo Collaboration. 2019, *GRB Coordinates Network, Circular Service*, No. 25324, 5324. <http://adsabs.harvard.edu/abs/2019GCN.25324....1L>
- Lipunov, V. M., Gorbovskoy, E., Kornilov, V. G., et al. 2017, *ApJ*, 850, L1. <https://doi.org/10.3847/2F2041-8213%2F20170411>
- Louis, T., Grace, E., Hasselfield, M., et al. 2017, *Journal of Cosmology and Astroparticle Physics*, 06, 031. <http://adsabs.harvard.edu/abs/2017JCAP...06..031L>
- Mandel, I., Farr, W. M., & Gair, J. R. 2019, *MNRAS*, 486, 1086. <http://arxiv.org/abs/1809.02063>

- Mortlock, D. J., Feeney, S. M., Peiris, H. V., Williamson, A. R., & Nissanke, S. M. 2019, *Physical Review D*, 100, 103523. <http://arxiv.org/abs/1811.11723>
- Nair, R., Bose, S., & Saini, T. D. 2018, *Physical Review D*, 98, 023502. <https://link.aps.org/doi/10.1103/PhysRevD.98.023502>
- Nissanke, S., Holz, D. E., Hughes, S. A., Dalal, N., & Sievers, J. L. 2010, *The Astrophysical Journal*, 725, 496. <http://arxiv.org/abs/0904.1017>
- Ossokine, S., Buonanno, A., Marsat, S., et al. 2020, arXiv e-prints, 2004, arXiv:2004.09442. <http://adsabs.harvard.edu/abs/2020arXiv200409442O>
- Palmese, A., deVicente, J., Pereira, M. E. S., et al. 2020, arXiv:2006.14961 [astro-ph]. <http://arxiv.org/abs/2006.14961>
- Planck Collaboration, Aghanim, N., Akrami, Y., et al. 2018, arXiv:1807.06209 [astro-ph]. <http://arxiv.org/abs/1807.06209>
- Riess, A. G. 2020, *Nature Reviews Physics*, 2, 10. <http://arxiv.org/abs/2001.03624>
- Riess, A. G., Casertano, S., Yuan, W., Macri, L. M., & Scolnic, D. 2019, 876, 85. <https://doi.org/10.3847%2F1538-4357%2Fab1422>
- Riess, A. G., Casertano, S., Yuan, W., et al. 2018, *ApJ*, 861, 126. <http://adsabs.harvard.edu/abs/2018ApJ...861..126R>
- Schechter, P. 1976, *ApJ*, 203, 297. <http://adsabs.harvard.edu/abs/1976ApJ...203..297S>
- Schutz, B. F. 1986, *Nature*, 323, 310. <https://www.nature.com/articles/323310a0>
- Shajib, A. J., Birrer, S., Treu, T., et al. 2020, *MNRAS*, staa828. <http://arxiv.org/abs/1910.06306>
- Soares-Santos, M., Holz, D. E., Annis, J., et al. 2017, *ApJ*, 848, L16. <http://arxiv.org/abs/1710.05459>
- Soares-Santos, M., Palmese, A., Hartley, W., et al. 2019, *ApJ*, 876, L7. <http://arxiv.org/abs/1901.01540>
- Story, K. T., Reichardt, C. L., Hou, Z., et al. 2013, *ApJ*, 779, 86. <http://arxiv.org/abs/1210.7231>
- Tanvir, N. R., Levan, A. J., Gonzalez-Fernandez, C., et al. 2017, *ApJ*, 848, L27. <https://doi.org/10.3847%2F2041-8213%2Faa90b6>
- Thrane, E., & Talbot, C. 2019, *Publications of the Astronomical Society of Australia*, 36, e010. <http://arxiv.org/abs/1809.02293>
- Valenti, S., Sand, D. J., Yang, S., et al. 2017, *ApJ*, 848, L24. <http://arxiv.org/abs/1710.05854>
- Veitch, J., Raymond, V., Farr, B., et al. 2015, *Physical Review D*, 91, 042003. <http://arxiv.org/abs/1409.7215>
- Verde, L., Treu, T., & Riess, A. G. 2019, *Nature Astronomy*, 3, 891. <http://arxiv.org/abs/1907.10625>
- Vitale, S. 2020, arXiv:2007.05579 [astro-ph, physics:gr-qc]. <http://arxiv.org/abs/2007.05579>
- Vitale, S., & Chen, H.-Y. 2018, *Physical Review Letters*, 121, 021303. <http://arxiv.org/abs/1804.07337>
- Wong, K. C., Suyu, S. H., Chen, G. C.-F., et al. 2019, arXiv:1907.04869 [astro-ph]. <http://arxiv.org/abs/1907.04869>